Mass Diffusion Effect in Large Zeolite Y Aggregates on Pd Cluster Size Distribution: A Combined in Situ EXAFS/XRD Study

W. Vogel

Fritz-Haber-Institut der Max-Planck-Gesellschaft, Faradayweg 4-6,14195 Berlin, Germany

H. Knözinger

Institut für Physikalische Chemie, Universität München, 80333 München, Germany

B. T. Carvill,† W. M. H. Sachtler, and Z. C. Zhang*,‡

Ipatieff Laboratory, Department of Chemistry, Northwestern University, Evanston, Illinois 60208

Received: October 22, 1997

EXAFS and XRD, the latter in the advanced mode of Debye function analysis (DFA), were combined to investigate the effect of preparation conditions on the size of Pd clusters inside the cavities of zeolite Y. It is concluded that the macroscopic size and extent of compactness of the sample exert a strong effect on the ultimate dispersion of the metal inside the zeolite. The rates of effective pore diffusion during the calcination of the ion-exchanged sample in a flow of oxygen are critical. Crucial is the composition of the local atmosphere, inside the zeolite cavities, at the stage when the ammine ligands of the $Pd(NH_3)_4^{2+}$ decompose. If mixing of the external, oxygen-rich atmosphere with the local reducing atmosphere is insufficient, "*autoreduction*" of Pd ions to Pd^0 takes place, and the primary clusters tend to agglomerate to large entities. When all other parameters are kept equal, the extent of mixing between local and external atmosphere will depend on the sample size and its degree of compactness. In the present work prepressed pellets are compared with zeolite powders. As expected, metal agglomeration is more pronounced in the former case, because mixing of the gases is less efficient and the local atmosphere remains reducing, thus favoring autoreduction of the Pd. Earlier findings that exposure to carbon monoxide induces secondary metal agglomeration are confirmed.

1. Introduction

Synthesis of metal clusters in zeolites with desired cluster size has led to a good understanding of the fundamental characteristics of bifunctional catalysts.[1,2] This knowledge provides a reliable basis for further catalyst design to achieve desired metal cluster sizes and controlled acidity.[3,4] For example, Pt and Pd clusters of various nuclearity including single atoms have been synthesized in zeolite pores and channels.[5−12]

During catalyst preparation, there are a number of factors that affect the ultimate particle size distribution. With a given zeolite structure, such parameters as pH and temperature of ion exchange,[13,14] metal precursors,[15] calcination temperature,[16] heating rate during calcination,[17] composition and flow rate of gas stream during calcination,[18−20] reduction temperature,[21] moisture level,[22] etc., are known to affect the size of metal particles in zeolites. The valence, reducibility, and size of other charge-compensating cations in the zeolite also dramatically control the location and particle size distribution of metals.[23,24]

Metal zeolite catalysts are usually prepared by starting with fine crystalline zeolite materials. Ion exchange in an aqueous slurry of microcrystalline zeolites is typically carried out to introduce ionic metal precursors into zeolite cavities. Subsequent treatments such as drying, calcination, and reduction are usually performed on powder samples. Conclusions reached from the laboratory samples in microcrystalline powder, however, may not apply to samples in large zeolite aggregates. The size of zeolite crystallites or aggregates should also be considered when comparing results from one batch to another.

Previous to characterization of metal zeolite catalysts in our laboratory, including EXAFS, samples were prepared using zeolite powder with crystallite size of a few microns. Complete pretreatment of zeolite powder samples preceded pelletization in a glovebox for EXAFS study. A high oxygen flow is required during calcination of amminated noble metal precursors in zeolites to minimize autoreduction which would lead to formation of large metal particles. Autoreduction will result from local oxygen deficiency which may be a consequence of a large mass diffusional gradient within a large aggregate. In the present study, the effect of large zeolite Y aggregates on the ultimate Pd particle size distribution was investigated by pretreating the catalyst precursor in the form of pellets, not a fine powder. The resulting metal clusters were characterized by combining in situ XRD and EXAFS. All other conditions were the same as previously used for powder samples.

Carbon monoxide was previously found to induce migration and coalescence of small primary Pd particles in zeolite cages

† Current address: Air Products and Chemicals, Inc., 7201 Hamilton Boulevard, Allentown, PA 18195.

‡ Current address: Akzo Nobel Chemical, Inc., 1 Livingstone Ave., Dobbs Ferry, NY 10522.

* To whom correspondence on this paper should be addressed.

S1089-5647(97)03430-5 CCC: $15.00
Published on Web 02/12/1998

at room temperature.[5] Therefore, it was also of interest to include CO-induced Pd particle agglomeration in the current study.

The technical advantages of both EXAFS and XRD are combined for a structural characterization of such metal/zeolite systems. The newly developed Debye function analysis (DFA)[25,26] for XRD is applicable to particle sizes below typically 35 Å, which are not detectable with conventional XRD. Moreover, DFA can provide information on metal particle size distributions. The sensitivity increases to the high end of this size range, while EXAFS is increasingly sensitive to the detection of clusters of low nuclearity.

Recently, there are concerns regarding the standard EXAFS evaluation of small metal particles on account of the anharmonicity effect.[27] The combination of XRD and EXAFS will minimize inaccuracies caused by this phenomenon.

2. Experimental Section

2.1. Sample Preparation. A batch of 9 wt % Pd/NaY was prepared by ion exchange of Na^+ at 24 °C with a solution of $Pd(NH_3)_4(NO_3)_2$. Details of the ion-exchange conditions are described elsewhere.[5] The batch was filtered and dried at 24 °C after exchange for 24 h. Two samples were prepared from the batch for parallel in situ XRD and EXAFS characterization. One was used to determine the variation of Pd cluster size at increasing reduction temperature from 200 to 400 °C. This sample is hereafter referred to as Pd/Y-T_R where T_R indicates the reduction temperature. Another sample was used to study the effect of CO on Pd nuclearity at increasing temperature from 15 to 45 °C after reduction at 200 °C in H_2. This sample will be referred to as Pd/Y-T_{CO} where T_{CO} is the temperature at which CO is admitted to the reduced sample. One hundred milligrams of both samples were first pelletized to a size of 8 × 15.5 mm from the batch of $Pd(NH_3)_4$/NaY saturated with ambient humidity. A 90 mg reference pellet, NaY (LZY-52, Union Carbide), was also used for parallel measurements.

2.2. System Setup. An in situ cell was used, which was originally designed for XRD measurements on a commercial Guinier powder diffractometer (HUBER).[25] The cell was mounted horizontally on a vertical goniometer (PICKER) by attaching to two $X-Y$ unislides placed on top of the Q axis. A special adapter allowed reproducible repositioning of the cell after a series of sample treatments outside the measurement hutch. A 2 mm entrance slit in combination with a 0.05 mrad soller slit was used in front of a NaI detector for the XRD measurements. All data were collected with constant I_0, monitored by an N_2 ionization chamber in the primary beam path. The XRD patterns were taken in transmission mode at an angle of 45° between the sample pellets and the primary beam. All 2Q scans were subdivided to a high-resolution low-angle scan and a normal-resolution wide-angle scan. In the XRD scan, one catalyst pellet and the pure NaY reference pellet were measured in parallel mode.

In the EXAFS mode the ionization chamber gas was changed to Ar. The 2Q arm was slewed to the zero position, and the NaI detector was replaced by a second ion chamber. All XRD and EXAFS scans were repeated at least twice.

As compared to previous XRD measurements using a commercial X-ray source and a Guinier powder diffractometer, the gain in intensity is approximately 2 orders of magnitude at CHESS. Nevertheless, the quality of the present data is lower, due to (i) a short beam-up time at CHESS and (ii) the 100 mg sample thickness being a compromise between the optimal value (∼30 mg) for XRD and the optimal value (∼200 mg) for EXAFS.

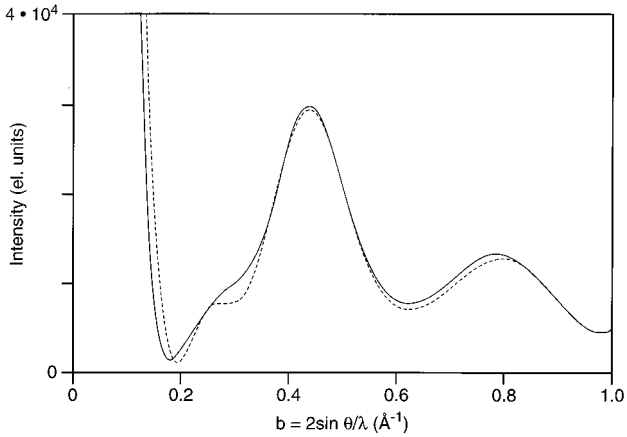

Figure 1. Debye functions of $Rh_{13}(CO)_{24}$ (solid line) and the same cluster with the CO ligands removed (dotted line).

2.3. Sample Pretreatment. In situ calcination was made in a flow of purified O_2 (>100 mL/min) to 400 °C for sample Pd/Y-T_R and to 430 °C for sample Pd/Y-T_{CO}, at a heating rate of 0.5 °C/min. The final calcination temperature was near the maximum temperature that the in situ cell could be safely operated. The samples were held at the final calcination temperature for 30 min before cooling to room temperature in O_2.

Reductions were performed outside the measurement hutch with a flow of purified H_2 by heating to T_R (°C) at a rate of 8 °C/min, holding for 20 min, and purging in He for 20 min before cooling to 24 °C in He. The reduction temperature was consecutively increased by 50 °C between measurements. Exposure to CO was performed by first cooling or heating to the desired temperature T_{CO} (°C) in He flow, followed by exposure to flowing CO for 20 min and purging with He for 20 min.

2.4. Measurement. Combined EXAFS and XRD data were collected at station C of the Cornell High Energy Synchrotron Source (CHESS). The ring energy is 5.25 GeV. The ring current was 80 mA at injection and decayed to 65 mA in about 50 min before dumping. A parallel cut Si-220 monochromator was used for EXAFS measurement at the Pd K-edge (24.34 keV). The same crystal was tuned to 10 keV for XRD measurement. In EXAFS measurement, the beam intensity was detuned by 30%.

2.5. Data Evaluation. *2.5.1. XRD.* It was shown in a previous paper[28] that X-ray interference terms between noble metal clusters and the host lattice of the support can in general be neglected due to the much larger scattering power of the metal atoms. Moreover, interference terms tend to cancel out in case of a random attachment of clusters to the support. Similarly, a CO coverage of the clusters in the case of carbonyl formation does not contribute noticeably to the intensity, at least in the wide-angle X-ray scattering (WAXS) range. This is demonstrated in Figure 1 by the Debye function of $Rh_{13}(CO)_{24}$, the X-ray structure of which has been described by Albano et al.,[29] and the corresponding Debye function of the naked Rh_{13} cluster, respectively.

The Debye function analysis (DFA) has been applied to extract information on the structure and size of metal particles.[25,26] Special data processing programs were developed to extract metal-phase intensity from the dominant signal of the zeolite host lattice. Palladium metal loading of less than 4 wt % is insufficient for a quantitative XRD analysis because of a low signal-to-noise ratio. In zeolite background subtraction, the X-ray pattern of the NaY reference sample was used to

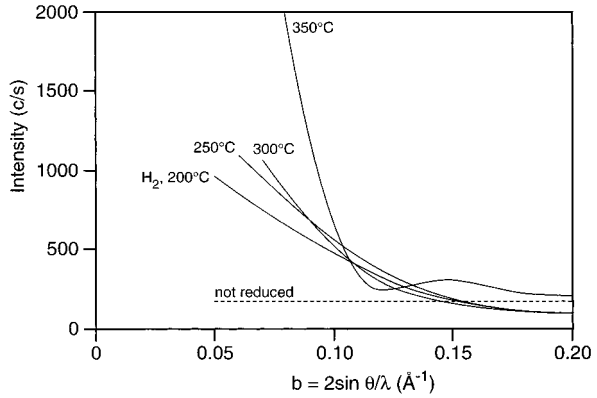

Figure 2. SAXS difference intensity for Pd/Y-T_R. The reduction temperatures (T_R) are labeled on the curves.

correct for (i) a scaling factor, (ii) line broadening, and (iii) line shifts in the metal-loaded zeolite due to lattice damages and expansion. It was noticed that in the calcined, dehydrated state the Pd/NaY unit cell was contracted by 0.5% compared to NaY and is still 0.3% smaller after reduction at 200 °C. Change of the unit cell size is known to occur as a function of cation exchange.[30]

The broad difference signal of the metal phase is generally superimposed by a high-frequency noise that is due to a slight shift in peak position and broadening of the zeolite diffraction peaks in the Pd/Y sample and the NaY reference.

A second method to extract the metal signal is to suppress all but the intensity values at the minima of the diffraction curve (MINIMA method). This method reduces the high-frequency noise but also reduces the total amount of information gained. This MINIMA method has some advantages, especially for the analysis of small-angle X-ray scattering (SAXS), extending to very strong zeolite peaks, the integral intensities of which are modified by ion exchange. Due to the extremely small metal particle sizes, the small-angle "shape scattering" extends to the WAXS range and can be alternatively included into the Debye function analysis. The difference intensity was corrected for absorption and geometric effects, including slit height correction in the small-angle range.

2.5.2. EXAFS. EXAFS data analysis was performed using a software package developed at the University of Washington and kindly provided by Professor Edward Stern. A thin film of Pd and a PdO pellet were used as reference materials. Details of data analysis have been reported previously.[5]

3. Results and Discussion

3.1. Influence of Reduction Temperature. The dependence of Pd particle size distribution on reduction temperature was studied between 200 and 400 °C. Figure 2 shows the difference intensities at different temperatures in the SAXS range for Pd/Y-T_R. In the unreduced state (dashed line) no small-angle scattering is visible. At reduction temperatures of 200, 250, and 300 °C, the intensities and slopes increased slightly with temperature, indicative of shape scattering by Pd particles. At 350 °C the SAXS increases steeply as a consequence of the onset of sintering of the palladium particles.

No noticeable amorphous phase caused by a breakdown of zeolite framework was observed. Therefore, the small-angle scattering could be included for simulations in addition to the intensity function in the range of WAXS. The calculated Debye functions were extended to the SAXS range. DFA was modified to include clusters Pd_N with nuclearities $N = 4$ and 6. For $N =$ 4 and 6 a regular tetrahedron and octahedron were assumed,

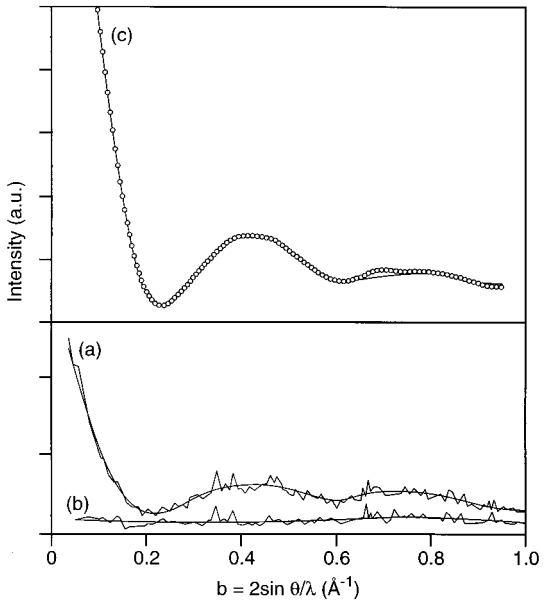

Figure 3. MINIMA filtered XRD data: (a) Pd/Y-T_R200, (b) NaY, and (c) difference intensity (circled point) and simulated intensity (solid line).

TABLE 1: DFA Results from XRD[a]

sample	Pd_4	Pd_6	Pd_{13}	Pd_{55}	$Pd_{N>55}$	⟨CN⟩	d_X
Reduced in Hydrogen at Increasing Temperature (T in °C following T_R)							
Pd/Y-T_R200	20	31	41	5	3	5	95
Pd/Y-T_R300	65	1	29	0	5	4.1	96
Pd/Y-T_R350		29	19	19	33	7.2	79
Pd/Y-T_R400	7	0	22	7	64	8.3	69
Exposure to CO at Increasing Temperature (T in °C following T_{CO})							
Pd/Y-T_{CO}15	26	52	21	0	1	4.1	98
Pd/Y-T_{CO}35	28	30	39	0	3	4.5	96
Pd/Y-T_{CO}45			∼60		∼40	∼8	∼60

[a] The numbers are the relative weight fractions of the corresponding clusters. ⟨CN⟩ and d_X are the weight-averaged coordination number and dispersion obtained from DFA.

respectively. Clusters Pd_N with $N = 13$ and 55 include both cuboctahedral and icosahedral shapes. Interaction with zeolitic oxygens and protons would not modify the scattering factor of Pd to a measurable extent, due to the low scattering power of these atoms. Even though the DFA could be modified to include $N = 1$, 2, and 3, these nuclearities are excluded from the fit since (i) scattering of monoatoms is hardly distinguishable from the background and (ii) the quality of the fit to the data will be sacrificed with a large set of free parameters.

The raw data in Figure 3, filtered by the MINIMA method, were obtained on sample Pd/Y-T_R200 (curve a) and on reference NaY (curve b). The NaY curve was multiplied with a proper absorption correction factor. The difference intensity (circles) and the simulated intensity (solid line) are shown in the same figure (curve c).

The fitted DFA results are listed in Table 1. The calculated average coordination numbers ⟨CN⟩ are also included in Table 1, i.e., the mass-weighted CN's of individual clusters. It must be noted that the individual weight values in Table 1 are subject to a high level of uncertainty.

The k^2-weighted EXAFS functions of the series Pd/Y-T_R reduced at 200, 300, 350, and 400 °C are displayed in Figure 4A, B, C, and D, respectively. Figure 4E is the EXAFS function of a reference Pd foil. The corresponding Fourier transforms

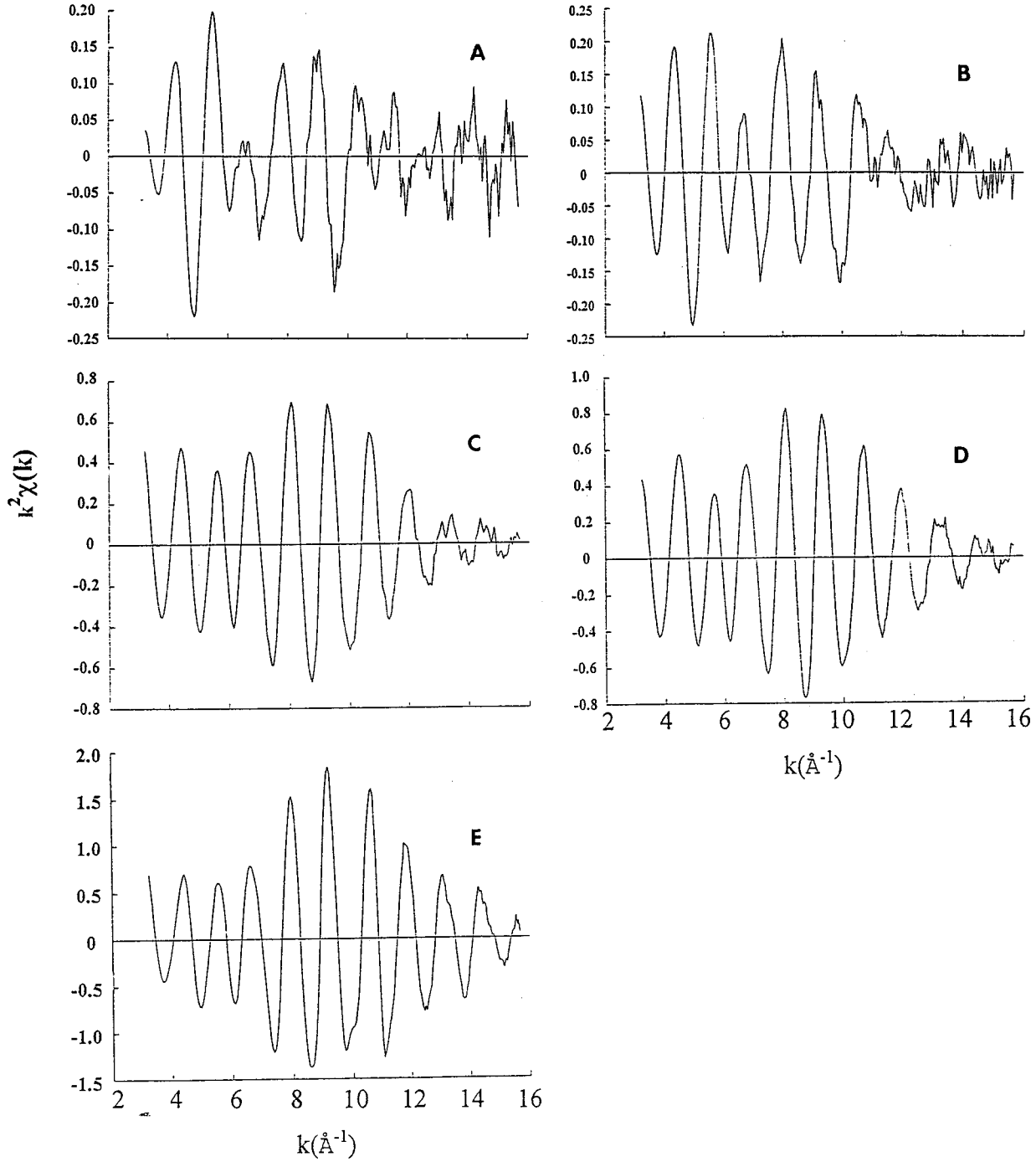

Figure 4. k^2-weighted EXAFS functions of Pd/Y-T_R with (A) T_R = 200, (B) 300, (C) 350, and (D) 400 °C. (E) Palladium reference foil.

within the k range 4−13 Å^{-1} are shown in Figure 5. Theoretical fits to the experimental data in the inverse Fourier transforms were performed on the Pd−Pd first shell between 2.1 and 2.9 Å, using Pd foil as a reference with the Pd−Pd first shell bond distance (R) of 2.74 Å and coordination number (CN) of 12. The fitted results are listed in Table 2. For clarity, the ⟨CN⟩ values of Table 1 are also listed in Table 2 so that the XRD and EXAFS results can be directly compared.

Both EXAFS CN and XRD ⟨CN⟩ results in Table 2 indicate that a large increase of Pd cluster size occurred at 350 °C. It must be pointed out again that EXAFS analysis is a more sensitive measure of lower Pd nuclearity (as are the cases for T_R = 200 and 300 °C) than XRD. On the other hand, better values are expected in XRD analysis of larger Pd nuclearity (as are the cases for T_R = 350 and 400 °C).

A major difference in Pd cluster size was found between Pd/Y-T_R of this work and similar samples studied previously.[5] In that earlier work, samples of exchanged Pd/Y powder were calcined and reduced in a sealed reactor before they were pelletized for EXAFS analysis. After reduction at 200 °C, the Pd was found to be monatomically dispersed. In the present study, calcination and reduction were performed on a pelletized sample. The average coordination number of 4.0 for Pd/Y-T_R200 is indicative of hexagonal clusters, which is in general agreement with the DFA analysis. The discrepancy in Pd cluster size as measured by EXAFS for powder samples and pellet samples is likely due to the presence of a large mass diffusional gradient from external surface of the pellet to the interior of the pellet. For loosely packed zeolite crystallites (powder samples), this effect was insignificant. As pointed out in the

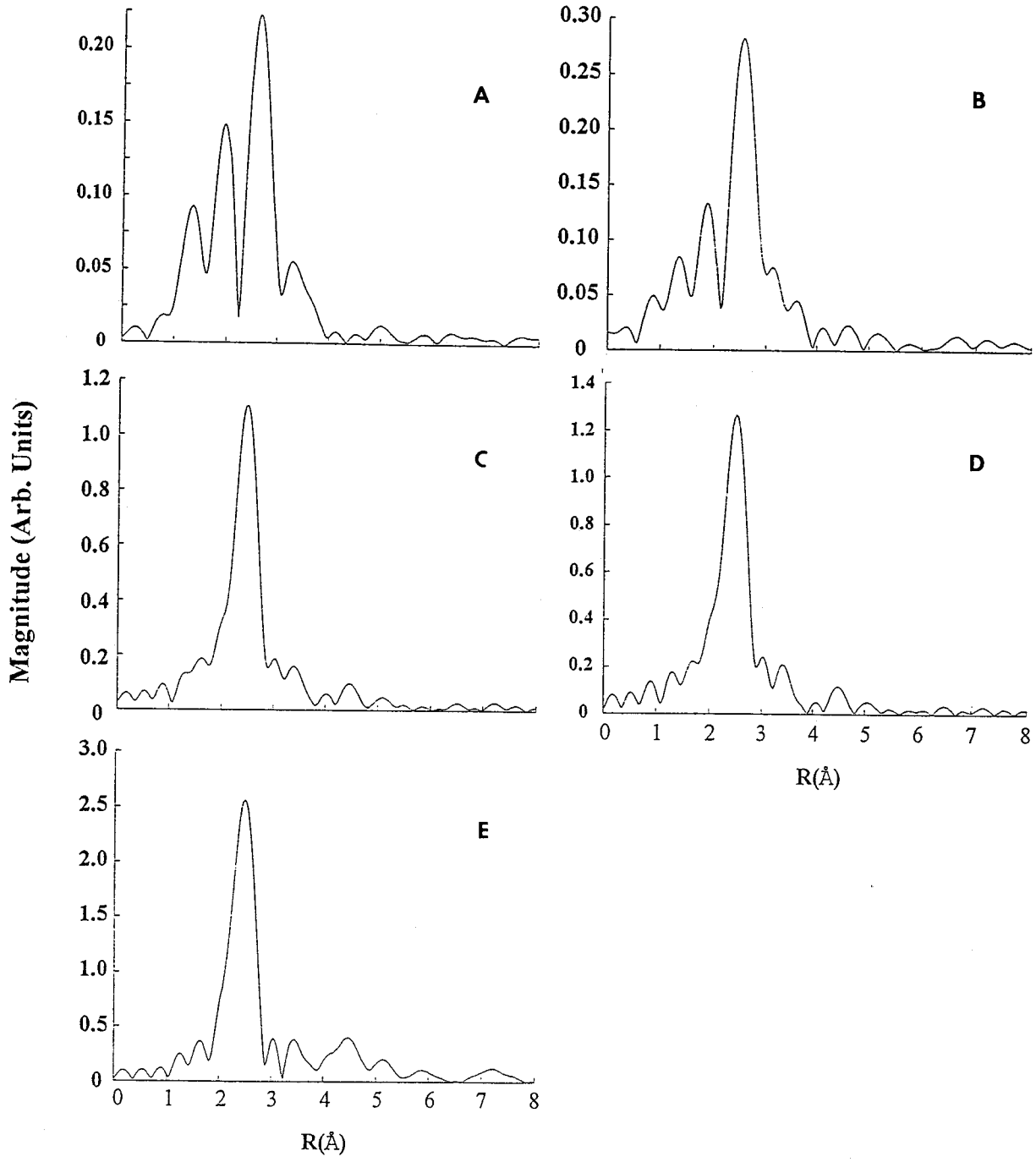

Figure 5. Fourier transforms corresponding to Figure 4 of Pd/Y-T_R with (A) $T_R = 200$, (B) 300, (C) 350, and (D) 400 °C. (E) Palladium reference foil.

TABLE 2: Fitted EXAFS Parameters for Sample Pd/Y-T_R Reduced at Different Temperatures

T_R (°C)	CN (EXAFS)	⟨CN⟩ (XRD)	R (Å)	$s \times 10^2$
200	4.0	5	2.83	0.80
300	4.6	4.1	2.77	0.93
350	8.6	7.2	2.72	0.36
400	8.7	8.3	2.72	0.26

Introduction, the rate of calcination has been found to be crucial for the ultimate Pd cluster size;[4] a faster heating rate leads to an increased Pd cluster size. This observation was mainly attributed to the autoreduction of amminated Pd precursors. The observed difference in Pd nuclearity between samples either in pelletized aggregates or in fine powder can also be attributed to the same cause. While a faster heating rate may create mass-transfer limitation within a single crystallite, a similar effect is also conceivable for zeolite aggregates densely pressed together into pellets with a dimension many orders of magnitude larger than a single zeolite grain. The reasonably good agreement between EXAFS and XRD measurements supports this conclusion. Meanwhile, the agreement between EXAFS and XRD measurement does not support the skepticism that EXAFS underestimates the coordination number in small metal clusters.

Upon increasing the temperature from 200 to 300 °C, the Pd cluster size as determined by EXAFS was slightly increased (Table 2). The XRD results in Table 1 suggest that XRD analysis for the samples reflected a larger error. However, a large increase in Pd nuclearity was observed at 350 °C, both by EXAFS and by XRD.

The one data point where the two methods differ significantly is Pd/Y-T_R200. According to the XRD data, ⟨CN⟩ is 5 for this

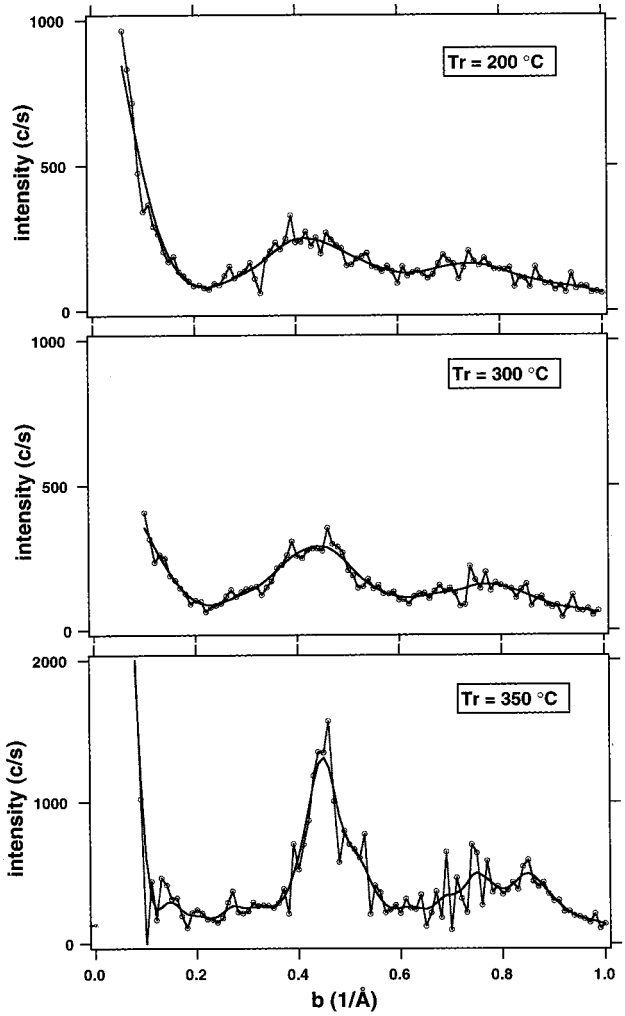

Figure 6. XRD difference intensity (MINIMA filtered) of Pd/Y-T_R with T_R = 200, 300, and 350 °C.

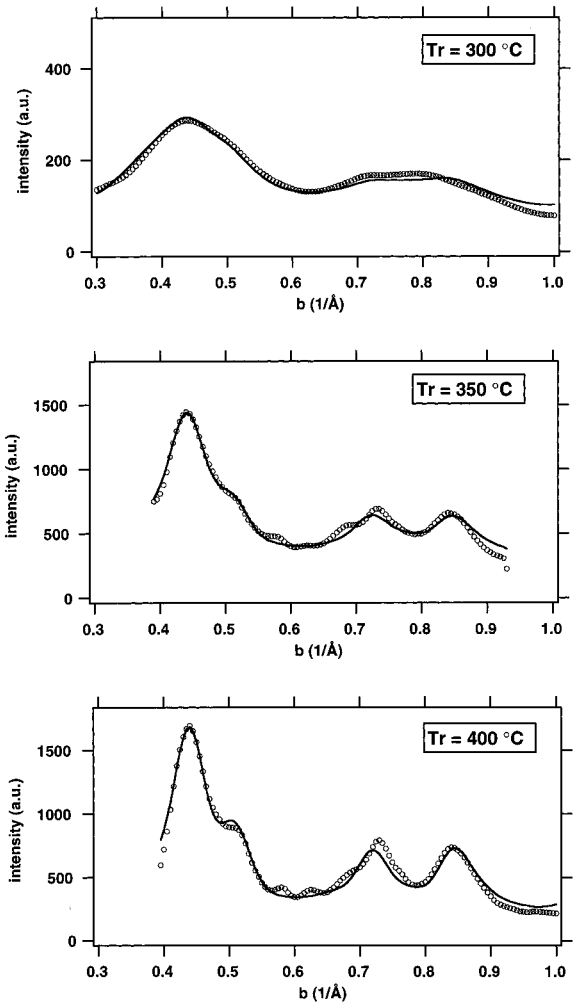

Figure 7. DFA simulation of MINIMA-filtered difference intensity of Pd/Y-T_R with T_R = 300, 350, and 400 °C.

sample. However, when the reduction temperature is increased to 300 °C, the coordination number determined by XRD decreases to 4.1. One possible explanation for this discrepancy is that particles containing fewer than four Pd atoms were excluded from the analysis because of the poor signal-to-noise ratio. After reduction at 200 °C, there are smaller particles that are left out the analysis. Reduction at higher temperature causes agglomeration of these particles to a size that can be captured by the XRD analysis. The EXAFS data, which are expected to be more accurate for the smaller particles produced at the lower reduction temperatures, support this theory by showing an increase in the CN from 4.0 to 4.6 with the increase in reduction temperature.

The large increase in Pd nuclearity at 350 °C is also evidenced by the difference intensity (MINIMA method) at different stages of reduction (Figure 6). The corresponding DFA simulations are displayed in Figure 7. The sharpening of the scattering curve at 350 and 400 °C clearly indicates a significant Pd particle agglomeration.

The standard DFA was applied to the WAXS intensity curves. Due to a high noise of the data, only the smoothed size distribution functions are evaluated. No attempt was made to distinguish individual icosahedral and cuboctahedral particles. The WAXS particle size distributions are shown in Figure 8. The larger particles formed at 350 and 400 °C show mainly fcc symmetry, which indicates fcc particles. Typical for these

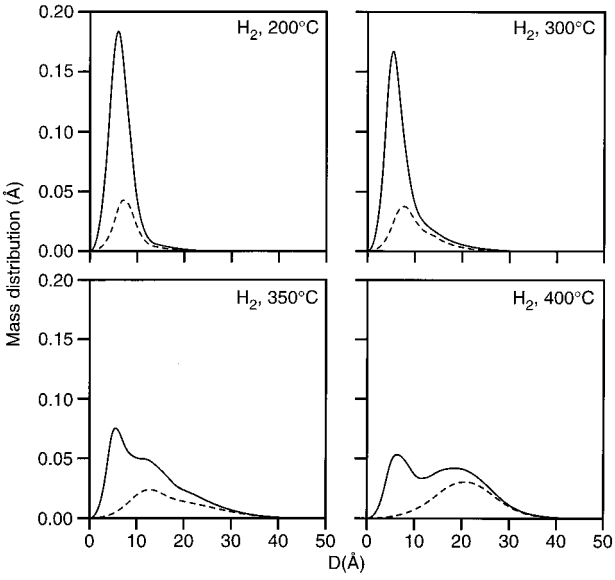

Figure 8. Normalized mass-weighted size distributions of Pd/Y-T_R with T_R = 200, 300, 350, and 400 °C obtained from WAXS. The dotted line represents the contribution of particles with fcc symmetry.

particles is the appearance of two maxima around the fcc Bragg peaks 220 and 311.

3.2. Agglomeration of Pd Primary Particles in CO. It was reported in a previous paper[5] that large Pd clusters were formed

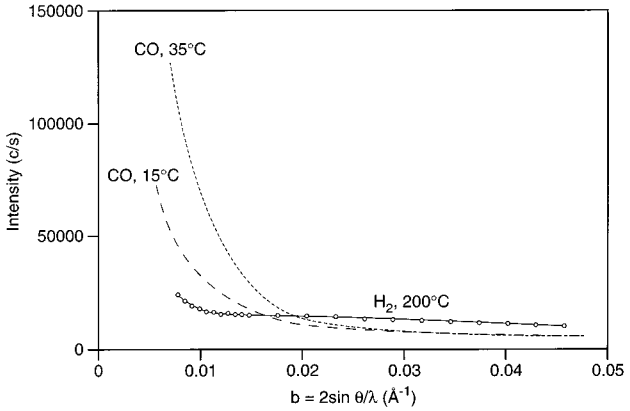

Figure 9. SAXS difference intensities of Pd/Y-T_R200, Pd/Y-T_{CO}15, and Pd/Y-T_{CO}35.

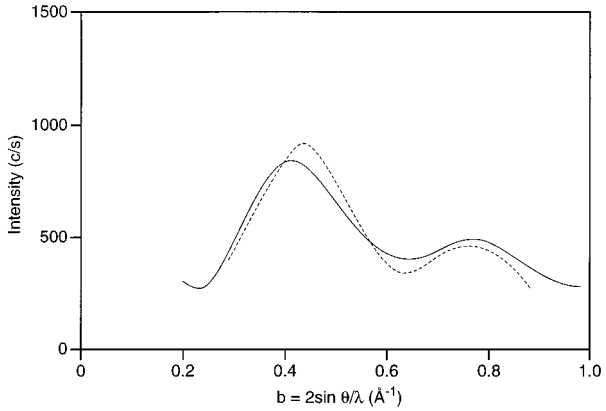

Figure 11. WAXS curves of Pd/Y-T_{CO}15 (solid line) and Pd/Y-T_R200 (dashed line).

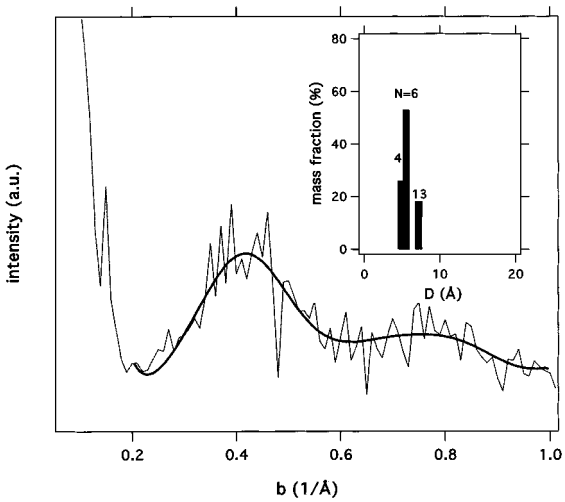

Figure 10. MINIMA-filtered WAXS difference intensity of Pd/Y-T_{CO}15. Thick solid line: FDA simulation. Inset: mass fractions of individual clusters Pd_N, $N = 4$, 6, and 13.

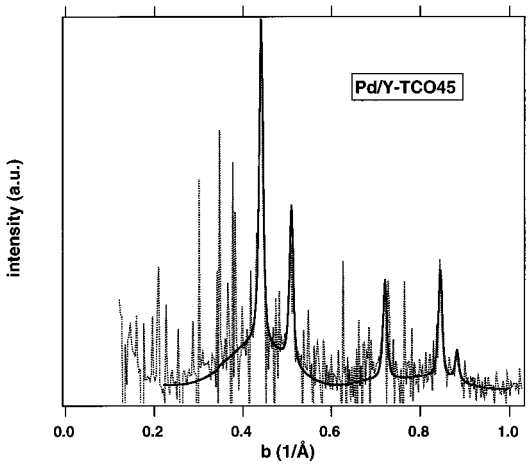

Figure 12. WAXS difference curve of Pd/Y-T_{CO}45 (dotted line). The solid line is a simulation using two different fcc palladium particles with diameters 7 Å (60 wt %) and 100 Å (40 wt %).

by exposing a Pd/Y-T_R200 to an atmosphere containing CO at room temperature. That experiment was performed ex situ; several days had elapsed after CO exposure before the EXAFS measurement took place. In the present work, the EXAFS and XRD evaluations were performed under nearly in situ conditions (with a negligibly short period of sample transfer from a treatment hood to the X-ray hutch). In addition, the temperature at which CO was introduced was progressively increased starting from below 0 °C, and EXAFS and XRD evaluations were taken at each temperature. It was found in repeated measurements that little change in Pd nuclearity took place at 0 °C (data not shown). An increase in Pd particle size was observed at 15 °C. Shown in Figure 9 are the SAXS intensities of Pd/Y-T_R200 and of Pd/Y-T_{CO} samples after subtraction of the background scattering. Exposure to CO at 15 °C induced an increase of the SAXS intensity next to the primary beam, indicating the formation of some larger Pd particles (long-dashed line). The average Guinier radius R_g can be estimated from the initial slope of the SAXS curve as 38 Å, corresponding to a sphere diameter $D_s = 96$ Å. R_g does not noticeably change by higher exposure temperatures. Exposure to CO at 35 °C clearly increases the fraction of the large particles (short-dashed curve).

However, interpretation of R_g should be done with caution as the particles are polydispersed and the lowest scattering angles are not available.

In Figure 10, the WAXS difference intensity after exposure to CO at 15 °C is given. The Pd signal is obtained by the MINIMA method. The DFA fit (smooth solid line) gives a good agreement with this curve, the majority of clusters being hexamers (∼52%). The cluster distribution is shown in the inset of the figure. The Pd−Pd distance increased by ∼3% against the bulk Pd for this fit. Figure 11 clearly shows the shift of the first maximum of the scattering curve after CO exposure (solid line) against that obtained on the freshly reduced sample (dashed line). This confirms the previous EXAFS work that indicated an increase of the average Pd−Pd distance upon exposure to CO.[5] Likewise, Albano et al.[29] found an average Rh−Rh distance of 2.794 Å for the $Rh_{13}H_2(CO)_{24}]^{3-}$ anion cluster, which is 3.9% larger than that of the bulk Rh.

In previous work[5] where a Pd/Y-T_R200 sample was exposed to CO ex situ at room temperature (∼24 °C), an increase of Pd coordination number from CN = 0 to CN = 6 was found. A coordination number of 6 was indicative of the formation of Pd_{13} clusters. In the present in situ study, a small increase in Pd cluster size occurred at 15 °C, as indicated by the small increase in Pd−Pd coordination number (4.5, EXAFS), and Pd_6 clusters (XRD) are prevailing.

Figure 12 shows the WAXS difference pattern of Pd/Y-T_{CO}45, i.e., after CO treatment at 45 °C. Narrow palladium Bragg peaks are clearly seen above the noise. But the background is still modulated by a diffuse scattering component produced by very small Pd particles. This bimodal state cannot be treated by the DFA method. Alternatively, the experimental data in Figure 12 were fitted assuming a mixture of two spherical palladium

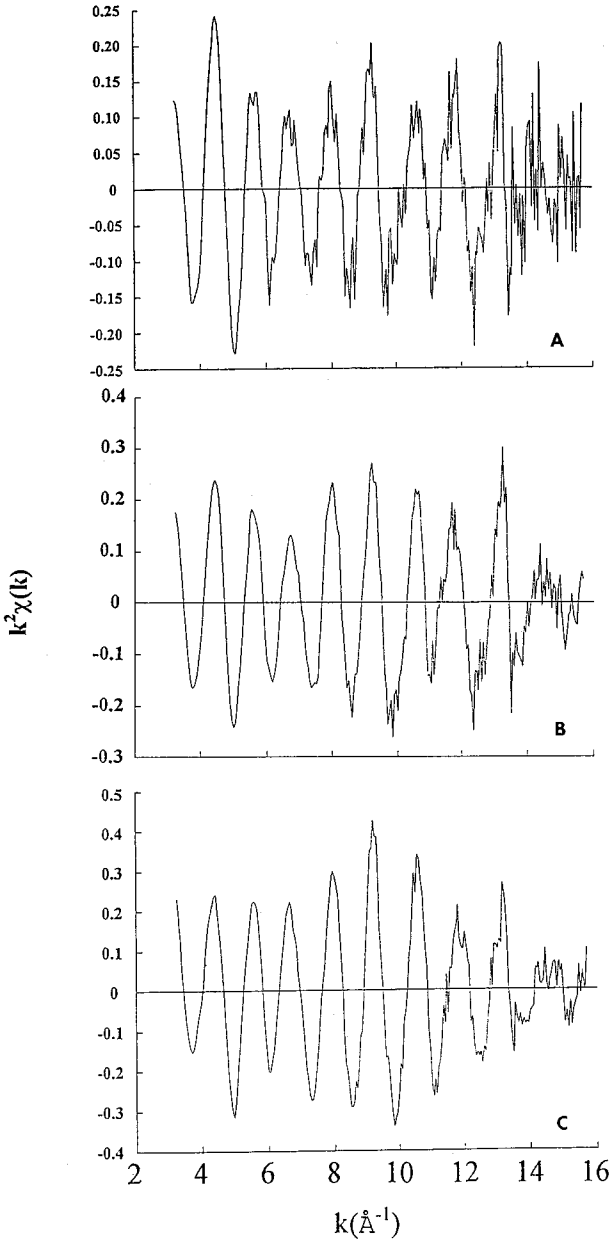

Figure 13. k^2-weighted EXAFS functions of Pd/Y-T_{CO}15, Pd/Y-T_{CO}35, and Pd/Y-T_{CO}45.

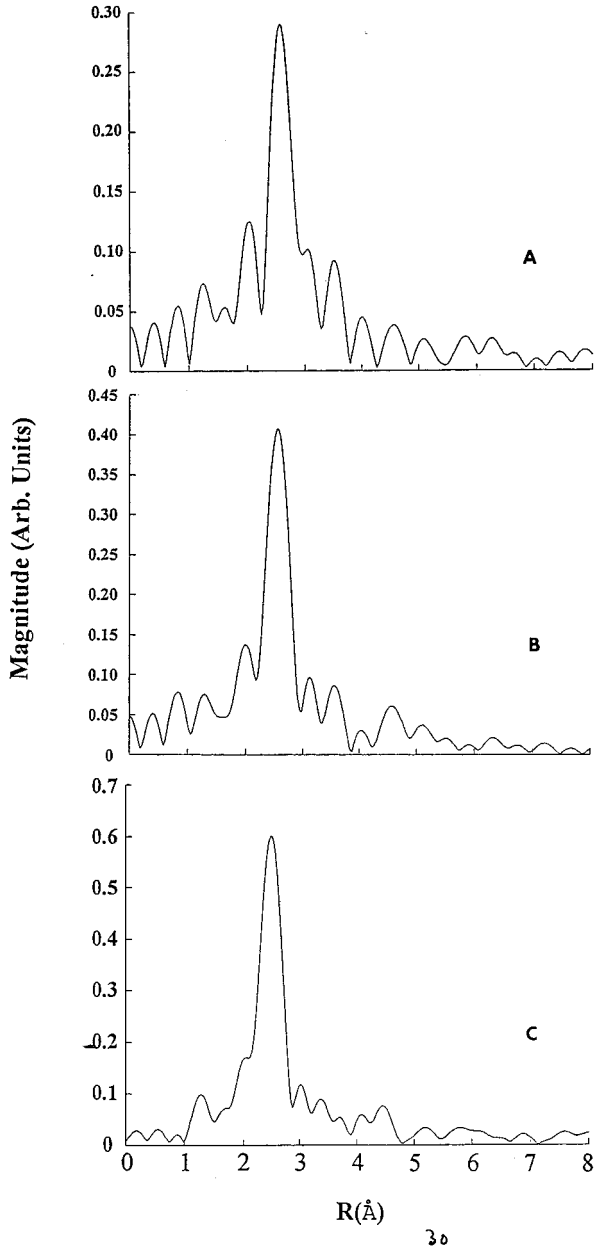

Figure 14. Fourier transforms corresponding to Figure 13 of Pd/Y-T_{CO}15, Pd/Y-T_{CO}35, and Pd/Y-T_{CO}45.

particles: (i) 60 wt % of 7 Å diameter and a second fraction of 40 wt % with 100 Å diameter.

The EXAFS analysis of the Pd/Y-T_{CO} is again in general agreement with that by XRD-DFA. The k^2-weighted EXAFS functions for the series Pd/Y-T_{CO}15, Pd/Y-T_{CO}35, and Pd/Y-T_{CO}45 are shown in Figure 13, A, B, and C, respectively. The corresponding Fourier transforms are displayed in Figure 14. Inspection of Figure 14 indicates the presence of some large Pd clusters as the Pd−Pd shells at distances beyond the first coordination shell are visible. Exposure to CO at lower temperature (15 °C) showed predominantly Pd−Pd in the first coordination shell.

The fitted EXAFS results for the series Pd/Y-T_{CO}, listed in Table 3, indicate a growth of Pd clusters with increasing temperature. The CN for Pd/Y-T_{CO}15 was slightly greater than that of the reduced sample. The growth at 35 and 45 °C was more pronounced, indicating that an optimum Pd cluster growth temperature in CO may be near or above room temperature. While XRD-DFA can provide an analysis of Pd particle size distribution, a general agreement was found between EXAFS and XRD for average Pd particle size determination.

TABLE 3: Fitted EXAFS Results for the Series Pd/Y-T_{CO}

T_{CO} (°C)	CN (EXAFS)	⟨CN⟩ (XRD)	R (Å)	$s \times 10^2$
15	4.5	4.1	2.77	0.92
35	5.1	4.5	2.77	0.74
45	7.5	8	2.75	0.50

4. Conclusions

After calcination and reduction under similar conditions, Pd particles in a pelletized Pd/Y zeolite are larger than those in fine Pd/Y zeolite powder from which the pellet was made. This observation is consistent with our previous results that local oxygen-rich atmosphere is essential during calcination in order to prevent *autoreduction* of $Pd(NH_3)_4^{2+}$ by rapidly decomposed ammine ligands. It was concluded in our previous study that a reduced oxygen concentration or a slightly accelerated temperature increase during calcination resulted in larger Pd particles

from $Pd(NH_3)_4^{2+}$/Y zeolite powder. It is shown in this work that autoreduction of $Pd(NH_3)_4^{2+}$ can also take place in a compressed sample due to ineffective diffusion of oxygen from the external atmosphere to the interior zeolite cavities where $Pd(NH_3)_4^{2+}$ ions are located.

In situ EXAFS and XRD (DFA) were combined to determine the effect of reduction temperature and CO atmosphere on the size of Pd clusters in Y zeolite. It was confirmed that the exposure of CO induces agglomeration of secondary Pd particles. The two techniques agree well at virtually all of the conditions tested. For very small particles (CN < 6), the EXAFS results appear to be more accurate, while for a distribution of larger particles, the XRD data yield better information.

Acknowledgment. We gratefully acknowledge a grant from NATO and financial support from the Director of the Chemistry Division, Basic Energy Sciences, U.S. Department of Energy (Grant DE-FG02-87ER13654). We thank Dr. Ken Finkelstein for his friendly help during our work at the synchrotron at CHESS, Cornell University.

References and Notes

(1) Sachtler, W. M. H. *Springer Ser. Surf. Sci.* **1990**, *22*, 69.
(2) Sachtler, W. M. H.; Zhang, Z. C. *Adv. Catal.* **1993**, *39*, 129.
(3) Zhang, Z. C.; Sachtler, W. M. H. *J. Mol. Catal.* **1991**, *67*, 349.
(4) Zhang, Z.; Cavalcanti, F. A.; Sachtler, W. M. H. *Catal. Lett.* **1992**, *12*, 157.
(5) Zhang, Z.; Chen, H.; Sachtler, W. M. H. *J. Chem. Soc., Faraday Trans. 1* **1991**, *87*, 1413.
(6) Sheu, L. L.; Knözinger, H.; Sachtler, W. M. H. *Catal. Lett.* **1989,** *2*, 129.
(7) Gallezot, P.; Alarcon-Diaz, A.; Dalmon, J. A.; Renouprez, A. J.; Imelik, B. *J. Catal.* **1975**, *39*, 334.
(8) Gallezot, P. *Catal. Rev.—Sci. Eng.* **1979**, *20* (1), 121.
(9) Bergeret, G.; Gallezot, P.; Imelik, B. *J. Phys. Chem.* **1981**, *85*, 411.
(10) Felthouse, T. R.; Murphy, J. A. *J. Catal.* **1986**, *98*, 411.
(11) Lerner, B. A.; Carvill, B. T.; Sachtler, W. M. H. *J. Mol. Catal.* **1992**, *77*, 99.
(12) Zholobenko, V. L.; Lei, G. D.; Carvill, B. T.; Lerner, B. A.; Sachtler, W. M. H. *J. Chem. Soc., Faraday Trans.* **1994**, *90* (1), 233.
(13) Stakheev, A. Y.; Khodakov, A. Y.; Kustov, L. M.; Kazansky, V. B.; Minachev, K. M. *Zeolites* **1992**, *12*, 866.
(14) Mirodatos, C.; Pichat, P.; Barthomeuf, D. *J. Phys. Chem.* **1976**, *80*, 1335.
(15) Zhang, Z.; Sachtler, W. M. H. *J. Chem. Soc., Faraday Trans.* **1990**, *86*, 2313.
(16) Tzou, M. S.; Sachtler, W. M. H. In *Catalysis 1987*; Ward, J. W., Ed.; Elsevier: Amsterdam, 1988; p 233.
(17) Zhang, Z.; Mestl, G.; Knözinger, H.; Sachtler, W. M. H. *Appl. Catal.* **1992**, *89*, 155.
(18) Verdonck, J.; Jacobs, P. A.; Genet, M.; Poncelet, G. *J. Chem. Soc., Faraday Trans.* **1980**, *74*, 403.
(19) Elliott, D. J.; Lunsford, J. H. *J. Catal.* **1979**, *57*, 11.
(20) Reagen, W. J.; Chester, A. W.; Kerr, G. T. *J. Catal.* **1981**, *69*, 89.
(21) Homeyer, S. T.; Sachtler, W. M. H. *J. Catal.* **1989**, *117*, 91.
(22) Yin, Y. G.; Zhang, Z.; Sachtler, W. M. H. *J. Catal.* **1993**, *139*, 444.
(23) Tzou, M. S.; Teo, B. K.; Sachtler, W. M. H. *J. Catal.* **1988**, *113*, 220.
(24) Zhang, Z.; Wong, T.; Sachtler, W. M. H. *J. Catal.* **1991**, *128*, 12.
(25) Vogel, W.; Sachtler, W. M. H.; Zhang, Z. *Ber. Bunsen-Ges. Chem. Phys.* **1993**, *97*, 280.
(26) Gnutzmann, V.; Vogel, W. *J. Phys. Chem.* **1990**, *94*, 4991.
(27) Hansen, L. B.; Stoltze, P.; Nørskov, J. K.; Clausen, B. S.; Niemann, W. *Phys. Rev. Lett.* **1990**, *64*, 3155.
(28) Vogel, W. *J. Catal.* **1990**, *121*, 356.
(29) Albano, V. G.; Ciani, G.; Martinengo, S.; Sironi, A. *J. Chem. Soc., Dalton Trans.* **1979**, 978.
(30) Fritz, P. O.; Lunsford, J. H.; Fu, C-.M. *Zeolites* **1988**, *8*, 205.